Measuring Squareness and Orientation of Shapes

Paul L. Rosin · Joviša Žunić

Abstract In this paper we propose a measure which defines the degree to which a shape differs from a square. The new measure is easy to compute and being area based, is robust – e.g., with respect to noise or narrow intrusions. Also, it satisfies the following desirable properties:
– it ranges over $(0, 1]$ and gives the measured squareness equal to 1 if and only if the measured shape is a square;
– it is invariant with respect to translations, rotations and scaling.

In addition, we propose a generalisation of the new measure so that shape squareness can be computed while controlling the impact of the relative position of points inside the shape. Such a generalisation enables a tuning of the behaviour of the squareness measure and makes it applicable to a range of applications. A second generalisation produces a measure, parameterised by δ, that ranges in the interval $(0, 1]$ and equals 1 if and only if the measured shape is a rhombus whose diagonals are in the proportion $1 : \delta$.

The new measures (the initial measure and the generalised ones) are naturally defined and theoretically well founded – consequently, their behaviour can be well understood.

As a by-product of the approach we obtain a new method for the orienting of shapes, which is demonstrated to be superior with respect to the standard method in several situations.

The usefulness of the methods described in the manuscript is illustrated on three large shape databases: diatoms (ADIAC), MPEG-7 CE-1, and trademarks.

Paul L. Rosin
School of Computer Science, Cardiff University, Cardiff CF24 3AA, Wales, U.K.
E-mail: Paul.Rosin@cs.cf.ac.uk

Joviša Žunić
Department of Computer Science, University of Exeter, Exeter EX4 4QF, U.K. and the Mathematical Institute, Serbian Academy of Arts and Sciences, Belgrade.
E-mail: J.Zunic@ex.ac.uk

1 Introduction

Shape descriptors are a powerful tool for shape classification tasks and many approaches have been developed [24]. There are a number of generic shape descriptors such as Fourier descriptors and moments that are capable of providing a high dimensionality feature vector that precisely describes specific shapes. Alternatively, other descriptors describe some single characteristic that is present over a variety of shapes, such as circularity [15], ellipticity, rectangularity, triangularity [17], rectilinearity [28], complexity [14] and symmetry [27]. Even for a single characteristic there often exist many alternative measures which are sensitive to different aspects of the shape, e.g. convexity [4,10,16,20,21,25,29]. Such a need for alternative measures is caused by the fact that there is no a single shape descriptor which is expected to perform efficiently in all possible applications – even the computation of perimeter is not a straightforward task [5,23].

In this paper we consider measuring a single, specific aspect of shape: squareness; i.e. how square is a shape? There appears to be little in the literature on methods to measure squareness beyond Bowman *et al.*'s [3] method. They describe the shape boundary by complex Fourier descriptors [8] $c_k = a_k + ib_k$ and use the normalised magnitude r_{-3}/r_1 to measure squareness, where $r_k = \sqrt{a_k^2 + b_k^2}$. A modified version was also given in Rosin [18].

In addition, there are some general approaches to defining shape descriptors that could be adopted to defining squareness [22]. For example, first, fit (somehow) a square $K_{fit}(S)$ to a measured shape S, and then estimate the squareness of the shape S by comparing $K_{fit}(S)$ and S. One straightforward possibility for a fitted square $K_{fit}(S)$ is the square whose centroid coincides with the centroid of S, whose area is equal to the area of S, and finally $K_{fit}(S)$ is rotated such that the area of $K_{fit}(S) \cap S$ is maximised. Now, a squareness measure (i.e. the comparison between S and $K_{fit}(S)$) can be given as

$$\mathcal{Q}_{fit}(S) \; = \; \frac{Area(S \cap K_{fit}(S))}{Area(S \cup K_{fit}(S))}. \tag{1}$$

Of course, there are other variations of this approach.

It is easy to check that the above defined squareness measure satisfies the following desirable properties:

(a') $\mathcal{Q}_{fit}(S) \in [0, 1]$;
(b) $\mathcal{Q}_{fit}(S) = 1$ if and only if S is a square;
(c) $\mathcal{Q}_{fit}(S)$ is invariant with respect to similarity transformations (i.e., translations, rotations and scaling);
(d) 0 is the best possible lower bound for $\mathcal{Q}(S)$ (i.e. the interval in **(a')** cannot be shortened).

Note. Notice that instead of the property $\mathcal{Q}_{fit}(S) \in [0, 1]$ in **(a')** we would prefer the following property to be satisfied:

(a) $\mathcal{Q}_{fit}(S) \in (0, 1]$.

That is, we would prefer that there is no shape with a positive area with measured squareness equal to 0. But, a (slight) disadvantage of the $\mathcal{Q}_{fit}(S)$ measure is that there are many shapes whose measured $\mathcal{Q}_{fit}(S)$ squareness is equal to 0. An example is a shape containing a large hole such that its intersection with the fitted square $K_{fit}(S)$ is empty.

In this paper we define a new squareness measure which satisfies the basic requirements **(a)**, **(b)**, **(c)** and **(d)**. A modification of the new measure is also described. Such a modification enables a control of the impact of the points' positions inside the measured shape to the computed squareness, and, consequently, enables a tuning of the behaviour of the squareness measure depending on the application where it is applied.

In comparison to the previously defined squareness measures [3,18] the proposed squareness measure can be applied to shapes represented either as boundaries or sets of internal pixels, and consequently is not restricted to single component shapes.

A by-product of squareness measures that are optimised over orientation, such as (1) above and the new measure which will be based on (19), is that they can be used to provide an estimate of shape orientation. There already exist various approaches to determine the orientation of shapes, the most common being the principal axis method, determined from the shape's moments [24]. While computing orientation of elongated shapes is straightforward, many approaches break down or become unreliable for compact and/or symmetric shapes [30]. It will be shown that our squareness based orientation estimate is more effective than the standard principal axis method in such circumstances.

The paper is organised as follows. The next section introduces the new squareness measure and proves several desirable properties of it. Section 3 gives some illustrative examples that demonstrate the behaviour of the new measure $\mathcal{Q}(S)$ and compare it with $\mathcal{Q}_{fit}(S)$.

In Section 4 we introduce a modification of $\mathcal{Q}(S)$ which gives different weights to the points inside the shape depending on their position with respect to the measured shape centroid. In such a way, the introduced squareness measure can be adopted to be successfully used in a wide range of applications. Illustrative examples and theoretical consideration of the modified measure are also given in Section 4. Section 5 uses the squareness measure for a variety of image processing applications. The suitability and effectiveness of all the method introduced by the paper are demonstrated on three large shape databases: diatoms (ADIAC), MPEG-7 CE-1, and trademarks. Comments and conclusions are in the last section.

2 Squareness Measure

In this section we define a squareness measure. Throughout the paper we assume that all shapes considered are planar and bounded. Moreover, since we are dealing with an area based shape measure, we will assume that all shapes, whose mutual set differences have their area equal to zero, are the same. We can formulate (mathematically) such a condition as

q1 All appearing shapes are bounded and if point A belongs to the considered shape S then there is a circle $C(A)$ with a small enough radius such that: $A \in C(A)$ and $C(A) \subset S$.

Clearly the condition **q1** is not a restriction in image processing and computer vision applications. For an area based descriptor, it is reasonable to expect that two objects

(shapes) whose symmetrical difference has zero area (e.g. two shapes whose difference consists of a finite number of isolated points or mathematically perfect lines whose width is zero) have the same measured value. For example, the open circle $\{(x, y) \mid x^2 + y^2 < 1\}$ and the closed circle $\{(x, y) \mid x^2 + y^2 \leq 1\}$ should have the same assigned measure if an area based descriptor is used. In this paper those two circles (the open one and the closed one) are assumed to be the same. In addition, the condition **q1** enables us to keep the proofs of Theorem 1 and Theorem 2 mathematically rigorous.

Also, any appearing shape will be considered to be positioned (translated) such that its centroid coincides with the origin, even if this is not explicitly stated.

We will use the l_1-distance in our derivation; the l_1-distance between points $A = (a_1, a_2)$ and $B = (b_1, b_2)$ is defined as:

$$l_1(A, B) = l_1((a_1, a_2), (b_1, b_2)) = |a_1 - b_1| + |a_2 - b_2|. \tag{2}$$

It is easy to see that the set of all points whose l_1-distance from the origin is smaller than r is a square. Such a square will be denoted by $K(r)$, i.e.

$$K(r) = \{(x, y) \mid |x| + |y| \leq r\}. \tag{3}$$

To define the new squareness measure, we start with the quantity

$$\min_{\alpha \in [0, 2\pi]} \iint\limits_{S(\alpha)} (|x| + |y|) dx dy \tag{4}$$

(where $S(\alpha)$ denotes the shape S rotated by an angle α around its centroid) and show that such a quantity reaches the minimum possible value if and only if S is a square. Exploiting this fact we will come to a new squareness measure. First, we prove the following theorem.

Theorem 1 *Let S be a given shape whose centroid coincides with the origin, and let $S(\alpha)$ denote the shape S rotated around the origin by an angle α. Then*

$$\frac{\iint_S (|x| + |y|) dx dy}{Area(S)^{3/2}} \geq \frac{\sqrt{2}}{3}; \tag{5}$$

$$\frac{\iint_S (|x| + |y|) dx dy}{Area(S)^{3/2}} = \frac{\sqrt{2}}{3} \quad \Leftrightarrow \quad S = K(r), \quad with \quad r = \frac{1}{\sqrt{2}} Area(S)^{1/2} \tag{6}$$

$$\frac{\min\limits_{\alpha \in (0, 2\pi]} \iint\limits_{S(\alpha)} (|x| + |y|) dx dy}{Area(S)^{3/2}} = \frac{\sqrt{2}}{3} \quad \Leftrightarrow \quad S \ \ is \ a \ square. \tag{7}$$

Proof. Let S be a shape as in the statement of the theorem. Also, let K, for short, denote the square $K\left(r = \frac{1}{\sqrt{2}} Area(S)^{1/2}\right)$ (i.e. the vertices of K are: $\left(\frac{1}{\sqrt{2}} Area(S)^{1/2}, 0\right)$, $\left(0, \frac{1}{\sqrt{2}} Area(S)^{1/2}\right)$, $\left(-\frac{1}{\sqrt{2}} Area(S)^{1/2}, 0\right)$, and $\left(0, -\frac{1}{\sqrt{2}} Area(S)^{1/2}\right)$ (see Fig.1). Trivially, the areas of S and K are the same, and also:

(i) The areas of the set differences $S \setminus K$ and $K \setminus S$ are the same (because the areas of S and K are the same);

(ii) The points from $K \setminus S$ are closer (in terms of l_1-distance) to the origin than the points from $S \setminus K$. I.e., more formally: If $(u, v) \in S \setminus K$ and $(w, z) \in K \setminus S$ then $|u| + |v| > |w| + |z|$ (see Fig. 1).

Further, (i) and (ii) give:

$$\iint\limits_{S \setminus K} (|x| + |y|) \ dx \ dy \ \geq \ \iint\limits_{K \setminus S} (|x| + |y|) \ dx \ dy. \qquad (8)$$

Now, we derive:

$$\iint\limits_{S} (|x| + |y|) dx dy$$

$$= \iint\limits_{S \setminus K} (|x| + |y|) dx dy + \iint\limits_{S \cap K} (|x| + |y|) dx dy$$

$$\geq \iint\limits_{K \setminus S} (|x| + |y|) dx dy + \iint\limits_{S \cap K} (|x| + |y|) dx dy$$

$$= \iint\limits_{K} (|x| + |y|) dx dy \ = \ \frac{\sqrt{2}}{3} Area(K)^{3/2} \ = \ \frac{\sqrt{2}}{3} Area(S)^{3/2}$$

which proves (5).
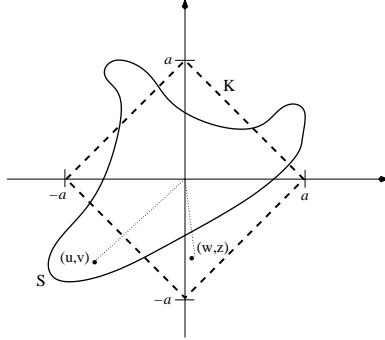
Fig. 1 Areas of S and $K = K \left(\frac{1}{\sqrt{2}} Area(S)^{1/2} \right)$ are the same (i.e. $a = \frac{1}{\sqrt{2}} Area(S)^{1/2}$). Each point (w,z) from $K \setminus S$ is closer to the origin than any point (u,v) from $S \setminus K$.

The statement (6) follows from the fact that the equality in (8) holds if and only if $Area(S \setminus K) = Area(K \setminus S) = 0$. I.e. shapes S and K are the same (here we need condition **q1**).

To prove (7), let α_0 be the angle for which $\iint_{S(\alpha)} (|x| + |y|) dx dy$ reaches the minimum. I.e.

$$\iint\limits_{S(\alpha_0)} (|x| + |y|) dx dy \ = \ \min_{\alpha \in (0, 2\pi]} \iint\limits_{S(\alpha)} (|x| + |y|) dx dy. \qquad (9)$$

Since

$$\frac{\min\limits_{\alpha\in(0,2\pi]}\int\int\limits_{S(\alpha)}(|x|+|y|)dxdy}{Area(S)^{3/2}} \;=\; \frac{\sqrt{2}}{3}$$

is assumed, and since $Area(S) = Area(S(\alpha)) = Area(S(\alpha_0))$ we obtain

$$\frac{\int\int\limits_{S(\alpha_0)}(|x|+|y|)dxdy}{Area(S(\alpha_0))^{3/2}} \;=\; \frac{\sqrt{2}}{3}. \tag{10}$$

Finally, accordingly to (6), shapes $S(\alpha_0)$ and K, are the same, i.e. S must be a square.
$\square$

Thus, Theorem 1 says that $\min\limits_{\alpha\in[0,2\pi)}\int\int_{S(\alpha)}(|x|+|y|)dxdy/Area(S)^{3/2}$ reaches the minimal possible value $\sqrt{2}/3$ if and only if S is a square. Based on this, we give the following definition.

Definition 1 Let S be a given shape. Then the squareness measure $\mathcal{Q}(S)$ is defined as

$$\mathcal{Q}(S) \;=\; \frac{\sqrt{2}}{3}\cdot\frac{Area(S)^{3/2}}{\min\limits_{\alpha\in[0,2\pi]}\int\int\limits_{S(\alpha)}(|x|+|y|)dxdy}, \tag{11}$$

where $S(\alpha)$ denotes the shape S rotated by an angle α around its centroid.

Theorem 2 summarises the desirable properties of $\mathcal{Q}(S)$.

Theorem 2 *The squareness measure $\mathcal{Q}(S)$ satisfies:*

(a) $\mathcal{Q}(S) \in (0,1]$, *for all shapes S;*
(b) $\mathcal{Q}(S) = 1 \quad\Leftrightarrow\quad S$ *is a square;*
(c) $\mathcal{Q}(S)$ *is an invariant w.r.t. similarity transformations;*
(d) *For each $\delta > 0$ there is a shape S such that $0 < \mathcal{Q}(S) < \delta$;*
    (i.e. 0 is the best possible lower bound for $\mathcal{Q}(S)$).

Proof. Items **(a)** and **(b)** follow directly from Theorem 1.

Item **(c)** follows from the fact that the quantities $\min\limits_{\alpha\in[0,2\pi]}\int\int_{S(\alpha)}(|x|+|y|)dxdy$ and $Area(S)$ do not depend on the rotation of S. So, $\mathcal{Q}(S)$ is rotationally invariant. $\mathcal{Q}(S)$ is translation invariant by definition which assumes that the centroid of S is always coincident with the origin. Finally, if shape S is dilated by a factor $\mathbf{r}$ to the shape $\mathbf{r}\cdot S$ then

$$\min\limits_{\alpha\in[0,2\pi]}\int\int\limits_{\mathbf{r}\cdot S(\alpha)}(|x|+|y|)dxdy \;=\; \mathbf{r}^3\cdot\min\limits_{\alpha\in[0,2\pi]}\int\int\limits_{S(\alpha)}(|x|+|y|)dxdy, \qquad Area(\mathbf{r}\cdot S) = \mathbf{r}^2\cdot Area(S)$$

and, consequently,

$$\mathcal{Q}(\mathbf{r}\cdot S) \;=\; \frac{\sqrt{2}}{3}\cdot\frac{Area(\mathbf{r}\cdot S)^{3/2}}{\min\limits_{\alpha\in[0,2\pi]}\int\int\limits_{\mathbf{r}\cdot S(\alpha)}(|x|+|y|)dxdy} \;=\; \frac{\sqrt{2}}{3}\frac{Area(S)^{3/2}}{\min\limits_{\alpha\in[0,2\pi]}\int\int\limits_{S(\alpha)}(|x|+|y|)dxdy} \;=\; \mathcal{Q}(S).$$

In other words, $\mathcal{Q}(S)$ is a scaling invariant as well.

To prove (**d**), let us consider a rectangle P_t whose vertices are $(t, -1)$ $(t, 1)$, $(-t, 1)$, $(-t, -1)$. By using the following

$$|x| + |y| \geq \sqrt{x^2 + y^2}, \qquad \iint\limits_{P_t(\alpha)} \sqrt{x^2 + y^2} dx dy = \iint\limits_{P_t} \sqrt{x^2 + y^2} dx dy \quad \text{(for all } \alpha\text{)}$$

we derive:

$$\mathcal{Q}(P_t) = \frac{\sqrt{2}}{3} \cdot \frac{Area(P_t)^{3/2}}{\min\limits_{\alpha \in [0,2\pi)} \iint\limits_{P_t(\alpha)} (|x| + |y|) dx dy} \leq \frac{\sqrt{2}}{3} \cdot \frac{Area(P_t)^{3/2}}{\iint\limits_{P_t(\alpha)} \sqrt{x^2 + y^2} dx dy}$$

$$\leq \frac{\sqrt{2}}{3} \cdot \frac{Area(P_t)^{3/2}}{\iint\limits_{P_t} \sqrt{x^2} dx dy} = \frac{\sqrt{2}}{3} \cdot \frac{(4t)^{3/2}}{2t^2} = \frac{4\sqrt{2}}{3} \cdot \frac{1}{\sqrt{t}}. \tag{12}$$

Now, a trivial equality $\lim\limits_{t \to \infty} \mathcal{Q}(P_t) = 0$ completes the proof. $\qquad \square$

Remark. Note that the obtained estimate $\lim\limits_{t \to \infty} \mathcal{Q}(P_t) = 0$ is in accordance with our perception. Indeed, if $t \to \infty$ the rectangle P_t degenerates into an infinitely long (but with constant width) strip and it is expected that the measured squareness $\mathcal{Q}(S)$ of such a shape tends to 0.

However, note also that there are many other shapes, different from very elongated rectangles whose measured squareness $\mathcal{Q}(S)$ can also be arbitrarily close to zero. For example, let us consider the circular ring C_r determined by the circles $x^2 + y^2 = (r+1)^2$ and $x^2 + y^2 = r^2$. Then,

$$\mathcal{Q}(C_r) = \frac{\sqrt{2}}{3} \cdot \frac{Area(C_r)^{3/2}}{\min\limits_{\alpha \in [0,2\pi)} \iint\limits_{C_r(\alpha)} (|x| + |y|) dx dy} = \frac{\sqrt{2}}{3} \cdot \frac{((2r+1)\pi)^{3/2}}{\iint\limits_{C_r} (|x| + |y|) dx dy}$$

$$= \frac{\sqrt{2}}{3} \cdot \frac{((2r+1)\pi)^{3/2}}{4 \cdot \int_{\varphi=0}^{\pi/2} \left(\int_{\rho=r}^{r+1} \rho^2 (\cos\varphi + \sin\varphi) d\rho \right) d\varphi} = \frac{((2r+1)\pi)^{3/2}}{2\sqrt{2}(3r^2 + 3r + 1)}. \tag{13}$$

Thus, the estimate (13) easily gives $\lim\limits_{r \to \infty} \mathcal{Q}(C_r) = 0$, i.e. very narrow circular rings can have an arbitrarily small measured squareness $\mathcal{Q}(S)$.

We compute $\mathcal{Q}(S)$ numerically by directly rotating and analysing each pixel in the shape, which is both straightforward and reasonably efficient. Optimisation is initially applied exhaustively over $[0, \frac{\pi}{2})$ at increments of 0.01 radians, and this approximate solution θ' is refined at increments of 0.001 radians over $[\theta' - 0.001, \theta' + 0.001]$. For example, the shapes in the MPEG-7 CE-1 database used in section 5 on average contain about 125,000 pixels (after normalisation), and the average computation time of $\mathcal{Q}(S)$ coded in C on a 2.0 GHz Pentium 4 was 0.16 seconds per shape.

Alternatively, the integrals could be evaluated directly from the shape boundaries which can reduce time complexity. If S is represented by a polygon then $\mathcal{Q}(S)$ can be computed in a convenient way using standard polygon operations, namely clipping and the computation of area and centroid. Considering just integrating $|x|$, the polygon is split into two parts: the positive X side P_{x+}, and the negative X side P_{x-}. Each of

the sides may consist of multiple disconnected polygons. Since $\int\limits_{P_{x+}}\int |x|dxdy = \bar{x}_{x+} \cdot Area(P_{x+})$, then

$$\int\limits_{S(\alpha)}\int (|x|+|y|)dxdy = \bar{x}_{x+}\cdot Area(P_{x+})-\bar{x}_{x-}\cdot Area(P_{x-})+\bar{y}_{y+}\cdot Area(P_{y+})-\bar{y}_{y-}\cdot Area(P_{y-}).$$

Runtime using this approach reduced the average computation time to 0.05 seconds per shape when the raw boundaries were first simplified by a moderate amount to contain on average 57 line segments.

3 Experiments Illustrating $\mathcal{Q}(S)$ Behaviour

To demonstrate the squareness measure it is applied to several image data sets. The first contains 808 *diatoms*, a type of unicellular algae [7]. The shapes minimising and maximising $\mathcal{Q}(S)$ are shown along with a range of other shapes spanning the measure's values (see figure 2). Since the range of diatom shapes is fairly restricted, decreasing values of squareness effectively correspond to increasing linearity of the shape. This is in accordance with the remark in the previous section that the measured squareness of infinitely long rectangles tends to zero.

| 0.305 | 0.400 | 0.501 | 0.600 | 0.701 | 0.800 | 0.900 | 0.992 |
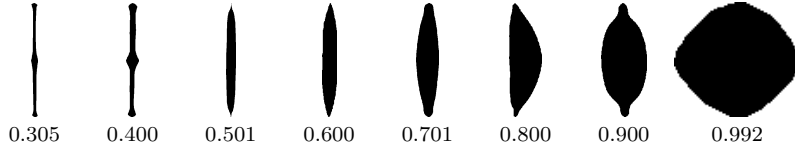
Fig. 2 Diatoms ranked by squareness $\mathcal{Q}(S)$.

| 0.325 | 0.366 | 0.370 | 0.371 | 0.375 | 0.377 | 0.377 | 0.378 | 0.378 | 0.385 |

| 0.452 | 0.501 | 0.550 | 0.605 | 0.658 | 0.702 | 0.750 | 0.800 | 0.850 | 0.900 |

| 0.998 | 0.998 | 0.999 | 0.999 | 0.999 | 0.999 | 1.000 | 1.000 | 1.000 | 1.000 |

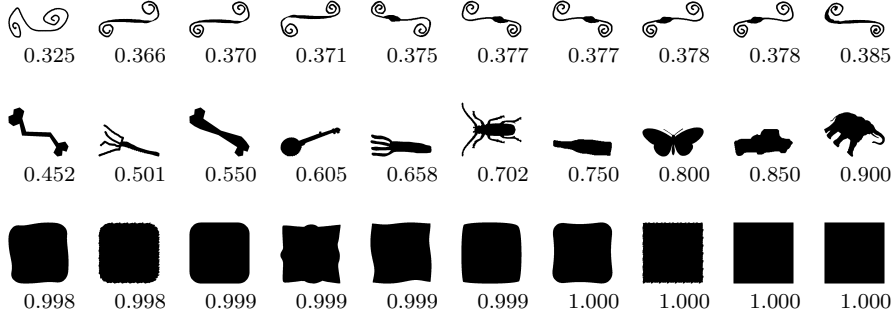**Fig. 3** MPEG-7 CE-1 shapes ranked by squareness $\mathcal{Q}(S)$.

The second database is the MPEG-7 CE-1 set of 1400 shapes. Figure 3 shows the ten highest and lowest ranked shapes according to squareness, plus ten intermediate shapes. The ten highest ranked shapes are indeed square, with varying degrees of irregularity
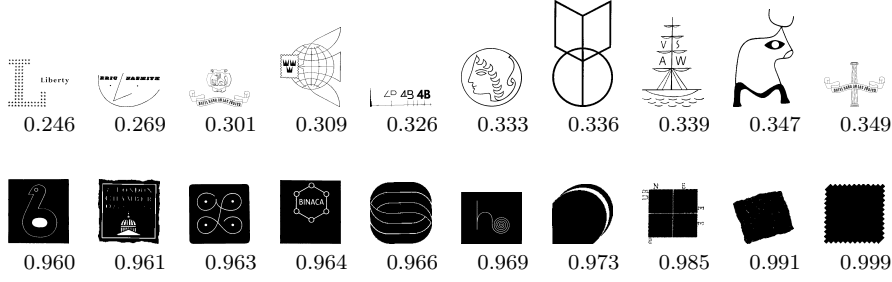
| 0.246 | 0.269 | 0.301 | 0.309 | 0.326 | 0.333 | 0.336 | 0.339 | 0.347 | 0.349 |

| 0.960 | 0.961 | 0.963 | 0.964 | 0.966 | 0.969 | 0.973 | 0.985 | 0.991 | 0.999 |

Fig. 4 Trademarks ranked by squareness $\mathcal{Q}(S)$.

(a) superellipse

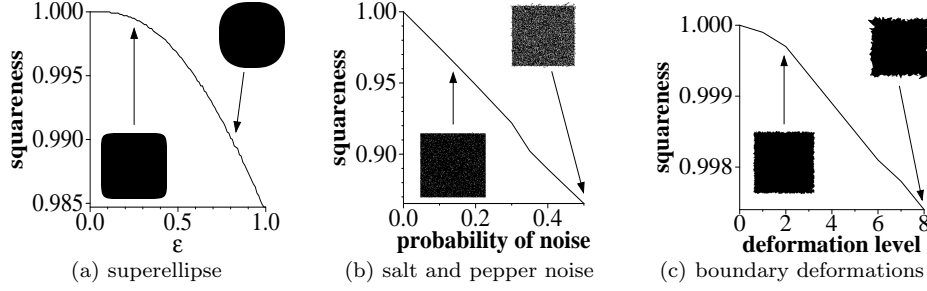(b) salt and pepper noise

(c) boundary deformations

Fig. 5 Increasing degrees of modification to a square cause a monotonic decrease in $\mathcal{Q}(S)$ for all three types of change in shape.

(bending, rounding, roughness). The ten lowest ranked shapes are not exactly linear, but their characteristics could be described as thin and elongated.

The third database contains 1100 trademarks which may consist of multiple components with holes [9]. The ten highest and lowest shapes ranked according to squareness are shown in figure 4. There is no simple perfect square in the database (this would not be a distinctive trademark), but the ten highest ranked shapes all have strong square-like characteristics. Again the ten lowest ranked shapes tend to contain thin and elongated features and are sparse (i.e. contain a large proportion of white pixels).

The squareness measure also exhibits intuitively reasonable behaviour. It has already been shown in (12) that for a rectangle $\mathcal{Q}(S)$ decreases as the rectangle becomes more elongated. Figure 5 provides further examples of the measure's correct behaviour in which $\mathcal{Q}(S)$ again decreases as the shape is modified from a perfect square. In figure 5a the superellipse, defined by the implicit equation $\left(\frac{x}{r}\right)^{\frac{2}{\epsilon}} + \left(\frac{y}{r}\right)^{\frac{2}{\epsilon}} = 1$, changes from a square (at $\epsilon = 0$) to a circle (at $\epsilon = 1$); in figure 5b increasing amounts of salt and pepper noise are added to the square; finally in figure 5c increasing amounts of deformations are added to the square's boundary. For the graphs in figure 5b and figure 5c $\mathcal{Q}(S)$ was averaged over 100 instances at each level of noise.

4 Point Position Dependent Squareness Measure

In this section we further develop our approach in order to enable some control of the impact of the relative positions of points inside the shape on the computed squareness.

Again, let S be a planar shape whose centroid coincides with the origin, and rotated such that $\iint_S (|x|+|y|)dxdy$ reaches its minimum. Then, informally speaking, two points $(x, y) \in S$ and $(\alpha x, \alpha y) \in S$ contribute to such an integral by $|x|+|y|$ and $|\alpha|(|x|+|y|)$ respectively, i.e., by their l_1-distances from the shape centroid. Obviously, for $|\alpha| < 1$ the point $(\alpha x, \alpha y)$ has a smaller impact on the minimised integral than the point (x, y). We could say that such an impact is smaller since $(\alpha x, \alpha y)$ is closer (also in sense of l_1-distance) to the centroid of S.

Such an impact of the shape point distances from the shape centroid (measured in the l_1-metric) to the optimising integral $\int\int_{S(\alpha)} (|x| + |y|)dxdy$ has a straightforward impact to the computed squareness $\mathcal{Q}(S)$.

The question is: *Is such an impact of the position of points, with respect to the shape centroid, always suitable or would we like to change it in some particular situations?*

For example, if we consider the measured $\mathcal{Q}(S)$ squareness of the elephant shape in second row in Fig.3 are we happy with such a relatively high measured squareness $\mathcal{Q}(S)$ which is 0.9002? Or, would we like the points which belong to the elephant's trunk (which are far from the shape's centroid) to have a higher impact and, in such a way, reduce the measured squareness?

In this section we give a modified method which allows us to control the impact of a point's position on the measured shape squareness, and in this way we enable a tuning of the behaviour of the squareness measure and make it more suitable in a wider range of applications than the initial squareness measure $\mathcal{Q}(S)$ introduced in Section 2.

We proceed with the following two lemmas which can be proven using the approach from the proof of Theorem 1.

Lemma 1 *Let S be a given shape whose centroid coincides with the origin, and let there be a constant $\beta > 0$. Then*

$$\frac{\min_{\alpha \in [0,2\pi]} \int_{S(\alpha)} \int (|x| + |y|)^\beta dxdy}{Area(S)^{1+\beta/2}} \geq \frac{2^{1-\beta/2}}{(\beta + 2)} \tag{14}$$

$$\frac{\min_{\alpha \in [0,2\pi]} \int_{S(\alpha)} \int (|x| + |y|)^\beta dxdy}{Area(S)^{1+\beta/2}} = \frac{2^{1-\beta/2}}{(\beta + 2)} \iff S \text{ is a square.} \tag{15}$$

Proof. Similarly as in the proof of Theorem 1, we consider the square $K(r)$ with $r = \sqrt{Area(S)/2}$ providing $Area(S) = Area(K(r))$. Also, centroids of S and $K(r)$ are assumed to be coincident. Then (see Fig.1), $\beta > 0$ implies:

$$(u, v) \in S \setminus K(r), \ (w, z) \in K(r) \setminus S \ \Rightarrow \ (|u| + |v|)^\beta > (|w| + |z|)^\beta,$$

which gives immediately:

$$\iint_{S \setminus K(r)} (|x| + |y|)^\beta \ dx \ dy \ \geq \ \iint_{K(r) \setminus S} (|x| + |y|)^\beta \ dx \ dy. \tag{16}$$

Now, we prove (14):

$$\iint\limits_{S} (|x| + |y|)^\beta \ dx \ dy$$

$$= \iint\limits_{S\setminus K(r)} (|x| + |y|)^\beta \ dx \ dy + \iint\limits_{S\cap K(r)} (|x| + |y|)^\beta \ dx \ dy$$

$$\geq \iint\limits_{K(r)\setminus S} (|x| + |y|)^\beta \ dx \ dy + \iint\limits_{S\cap K(r)} (|x| + |y|)^\beta \ dx \ dy$$

$$= \iint\limits_{K(r)} (|x| + |y|)^\beta \ dx \ dy \ = \ \frac{Area(S)^{1+\beta/2}}{2^{-1+\beta/2}(2+\beta)}.$$

To prove (15) is enough to notice that $S \neq K(r)$ would imply that the inequality (16) is strict. Consequently, S different from $K(r)$ gives

$$\iint\limits_{S} (|x| + |y|)^\beta \ dx \ dy \ > \ \iint\limits_{K(r)} (|x| + |y|)^\beta \ dx \ dy$$

for all shapes different from a square. □

Lemma 1 considers only $\beta > 0$, but it is also possible to consider negative β. To preserve the convergence of the integrals appearing we assume $\beta > -1$. Notice that, contrary to the situation when $\beta > 0$, in the case of $-1 < \beta < 0$ and S is a square, the quantity $\iint\limits_{S}(|x|+|y|)^\beta dxdy/(Area(S))^{1+\beta/2}$ reaches the maximal possible value. This maximal value is $2^{1-\beta/2}/(2+\beta)$. Taking this into account, the proof of the next lemma can be derived analogously to the proof of Lemma 1 and because of that it is omitted.

Lemma 2 *Let S be a given shape whose centroid coincides with the origin and let β be a constant such that $-1 < \beta < 0$. Then*

$$\frac{\max\limits_{\alpha\in[0,2\pi]} \iint_{S(\alpha)}(|x| + |y|)^\beta dxdy}{Area(S)^{1+\beta/2}} \leq \frac{2^{1-\beta/2}}{2+\beta} \tag{17}$$

$$\frac{\max\limits_{\alpha\in[0,2\pi]} \iint_{S(\alpha)}(|x| + |y|)^\beta dxdy}{Area(S)^{1+\beta/2}} = \frac{2^{1-\beta/2}}{2+\beta} \ \Leftrightarrow \ S \ is \ a \ square. \tag{18}$$

Now, by the arguments from Lemma 1 and Lemma 2 we give the following definition for a modified measure.

Definition 2 Let S be a given shape whose centroid coincides with the origin and a real β such that $-1 < \beta$ and $\beta \neq 0$. Then the squareness measure $\mathcal{Q}_\beta(S)$ is defined as

$$
\mathcal{Q}_\beta(S) = \begin{cases} \dfrac{2^{1-\beta/2} Area(S)^{1+\beta/2}}{(2+\beta) \min\limits_{\alpha \in [0,2\pi]} \iint_{S(\alpha)} (|x| + |y|)^\beta dxdy}, & \beta > 0 \\[20pt] \dfrac{(2+\beta) \max\limits_{\alpha \in [0,2\pi]} \iint_{S(\alpha)} (|x| + |y|)^\beta dxdy}{2^{1-\beta/2} Area(S)^{1+\beta/2}}, & \beta \in (-1,0) \end{cases} \tag{19}
$$

It is worth mentioning that such a generalised measure $\mathcal{Q}_\beta(S)$ still keeps the basic requirements that each squareness measure should have. We give the following theorem which summarises the desirable properties of $\mathcal{Q}_\beta(S)$. The proof is omitted because of the analogy with the proof of Theorem 2.

Theorem 3 *Let β be a real number, such that $\beta \neq 0$ and $\beta > -1$. Then, the squareness measure $\mathcal{Q}_\beta(S)$ satisfies the following properties:*

(a) $\mathcal{Q}_\beta(S) \in (0,1]$ *for all planar shapes S;*
(b) $\mathcal{Q}_\beta(S) = 1 \quad \Leftrightarrow \quad S$ *is a square;*
(c) $\mathcal{Q}_\beta(S)$ *is invariant w.r.t. the similarity transformations;*
(d) *For each $\delta > 0$ there is a shape S such that $0 < \mathcal{Q}_\beta(S) < \delta$.*

Since $\mathcal{Q}_{\beta=1}(S) = \mathcal{Q}(S)$ it is obvious that Definition 2 generalises Definition 1. Definition 2 allows the control of the behaviour of $\mathcal{Q}_\beta(S)$ by a suitable choice of β. The effect of altering β is demonstrated in figure 6. The trademarks used in figure 4 are re-ranked for various values of β. A negative $\beta = -0.5$ gives a lower measured squareness to the shape in figure 6(a3) than to the shape in figure 6(a4) while a small positive $\beta = 0.25$ changes the ranking among those two shapes (see shapes in figure 6(b4) and figure 6(b1)). Much larger β – i.e. $\beta = 4$ and $\beta = 16$ – do not even include the shape in figure 6(a4) (i.e. in figure 6(b1)) among the four highest ranked shapes from the database.

| 0.980 | 0.985 | 0.985 | 0.988 | | 0.995 | 0.996 | 0.998 | 1.000 |
| (a1) | (a2) | (a3) | (a4) | | (b1) | (b2) | (b3) | (b4) |

$$\beta = -0.5 \qquad\qquad\qquad \beta = 0.25$$

| 0.882 | 0.925 | 0.933 | 0.993 | | 0.624 | 0.626 | 0.636 | 0.918 |
| (c1) | (c2) | (c3) | (c4) | | (d1) | (d2) | (d3) | (d4) |

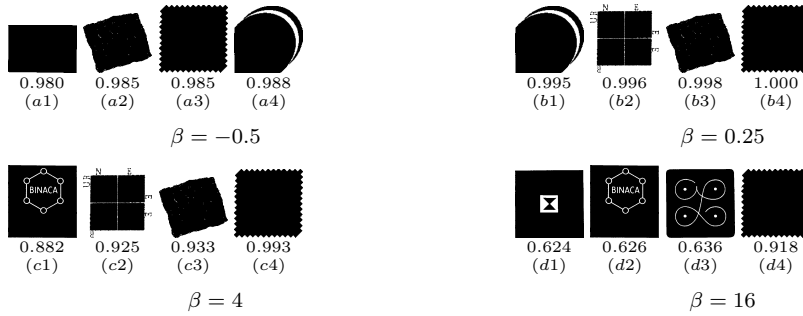$$\beta = 4 \qquad\qquad\qquad \beta = 16$$

Fig. 6 Four highest ranking trademarks according to $\mathcal{Q}_\beta(S)$ with different values of β.
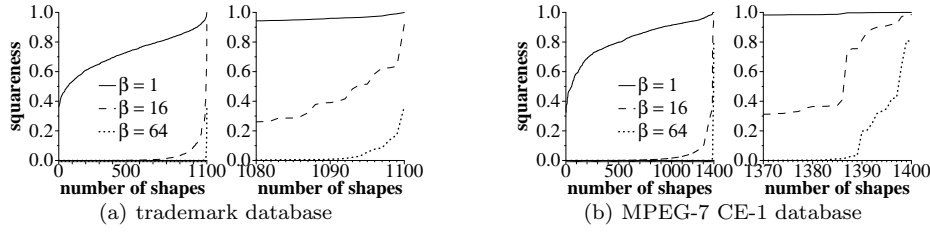
Fig. 7 Sorted squareness values ($\mathcal{Q}_{\beta=1}(S)$, $\mathcal{Q}_{\beta=16}(S)$ and $\mathcal{Q}_{\beta=64}(S)$) for the trademark and MPEG-7 CE-1 databases. With a large β value very few shapes have squareness values significantly larger than zero.

4.1 Behaviour of $\mathcal{Q}_\beta(S)$ for a large β

In this subsection we show that $\mathcal{Q}_\beta(S)$ strongly penalises even very small deviations of a shape S from a perfect square if β is chosen large enough. More formally, we prove that $\mathcal{Q}_\beta(S)$ tends to zero when β tends to infinity whenever S is different from a square. Of course, when S is a square then $\mathcal{Q}_\beta(S) = 1$ for all β. This is the statement of the following lemma whose proof is in the Appendix.

Lemma 3 *Let S be a shape different from a square. Then*

$$\lim_{\beta \to \infty} \mathcal{Q}_\beta(S) = 0. \tag{20}$$

The effect of large β is demonstrated on the trademark and MPEG-7 CE-1 databases, where high β can be used to penalise small irregularities from a square. Figure 7 shows cumulative distributions of the squareness values in the databases for various values of β; the rightmost graph of each pair in figure 7a and figure 7b shows a close-up of the top end of the distribution. As already seen in figure 4, there are no squares in the trademark database – all the trademarks have significant deviations either on the boundary or interior. The cumulative distribution in figure 7a therefore contains no large values of $\mathcal{Q}_{\beta=64}(S)$. The MPEG-7 CE-1 database contains a small number of fairly square-like shapes (about 10-20), and so there are several shapes with high squareness values, even for $\mathcal{Q}_{\beta=64}(S)$ – see figures 7b and 8. For both databases it can be seen that $\mathcal{Q}_{\beta=1}(S)$ is relatively large (e.g. > 0.5) for the majority of shapes. Increasing β to 16 generates a quicker drop-off in $\mathcal{Q}_{\beta=16}(S)$ for non-square shapes, and a further increase results in a sharp drop-off for $\mathcal{Q}_{\beta=64}(S)$.

The effect using large β is also visible when we consider the shapes in figure 8. All displayed shapes have a high squareness when measured by $\mathcal{Q}(S)$. Notice that even a circle has a high measured squareness if $\mathcal{Q}(S)$ is used – such a measured squareness is $\frac{\pi\sqrt{\pi}}{4\sqrt{2}} \approx 0.9844$. But, as mentioned above, if a higher β is used then the deviations from a square are penalised accordingly to the size of β selected. In the presented example $\beta = 64$ reduces all measured squareness. Despite that, all shapes in the second row could be understood as fairly square-like shapes, their measured $\mathcal{Q}_{\beta=64}(S)$ squareness ranges from 0.2031 to 0.8067 keeping a reasonable high measured squareness only for the last three shapes. The irregularities are bigger in the shapes in the first row and, because of that, the decrease in the measured squareness is much stronger. All obtained values are close to zero, including the measured $\mathcal{Q}_{\beta=64}(S)$ squareness for the circular shape which is 0.0023.
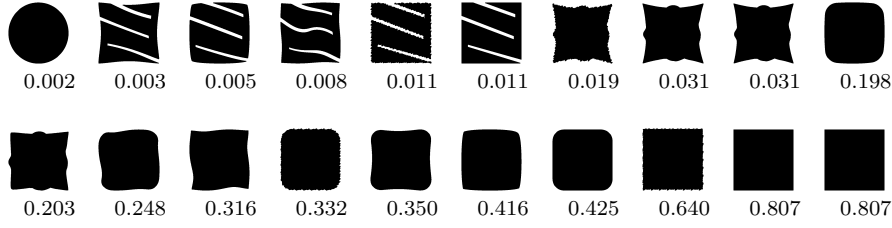
0.002 0.003 0.005 0.008 0.011 0.011 0.019 0.031 0.031 0.198

0.203 0.248 0.316 0.332 0.350 0.416 0.425 0.640 0.807 0.807

Fig. 8 Twenty highest ranking trademarks according to $\mathcal{Q}_{\beta=64}(S)$.

4.2 Modification for rhombus shapes

The method presented here to define the new squareness measure $\mathcal{Q}(S)$ allows several modifications. One such modification was introduced in Definition 2. It involves a parameter β, which enables a tuning of the behaviour of the squareness measure $\mathcal{Q}_\beta(S)$ enabling us to assign higher or lower weights to the points which are closer to the shape centroid. There is also a possibility for a further upgrade of the squareness measure $\mathcal{Q}_\beta(S)$. If we start from the set

$$R(r, \delta) = \{(x, y) \mid |x| + \delta \cdot |y| \le r\} \tag{21}$$

which is a rhombus (with vertices $(r, 0)$, $(0, r/\delta)$, $(-r, 0)$, and $(0, -r/\delta)$) for any choice of $\delta, r > 0$, (of course, it is a square if $\delta = 1$), and if we follow the same scenario as in developing the measures $\mathcal{Q}(S)$ and $\mathcal{Q}_\beta(S)$, we could come to a spectrum (depending on the selected δ) of rhomboidal measures $\mathcal{R}_\delta^\beta$. Those rhomboidal measures are precisely described by the following definition.

Definition 3 Let S be a given shape whose centroid coincides with the origin, β such that $-1 < \beta$ and $\beta \ne 0$ and $\delta > 0$. Then the rhomboidal measure $\mathcal{R}_\delta^\beta(S)$, which also incorporates the β weighting w.r.t. the distances of points from the origin, is defined as

$$\mathcal{R}_\delta^\beta(S) = \begin{cases} \dfrac{\delta^{\beta/2} \cdot (Area(S))^{(\beta+2)/2}}{(\beta + 2) \cdot 2^{(\beta-2)/2} \cdot \min\limits_{\alpha \in [0, 2\pi]} \iint_{S(\alpha)} (|x| + \delta \cdot |y|)^\beta \ dx \ dy}, & \beta > 0 \\[3em] \dfrac{(\beta + 2) \cdot 2^{(\beta-2)/2} \cdot \max\limits_{\alpha \in [0, 2\pi]} \iint_{S(\alpha)} (|x| + \delta \cdot |y|)^\beta \ dx \ dy}{\delta^{\beta/2} \cdot (Area(S))^{(\beta+2)/2}}, & \beta \in (-1, 0) \end{cases} \tag{22}$$

The new defined rhomboidal measure $\mathcal{R}_\delta^\beta(S)$ has all the desirable properties listed in Theorem 2 and Theorem 3 and satisfied by the measures $\mathcal{Q}(S)$ and $\mathcal{Q}_\beta(S)$. I.e., $\mathcal{R}_\delta^\beta(S)$ ranges in the interval $(0, 1]$ and equals 1 if and only if S is a rhombus whose diagonals are in the proportion $1 : \delta$. Also, $\mathcal{R}_\delta^\beta(S)$ is invariant with respect to similarity transformations. We leave to the reader to verify this.

The use of the modified measure $\mathcal{R}_\delta^\beta(S)$ to provide improvements over $\mathcal{Q}(S)$ and $\mathcal{Q}_\beta(S)$ in the estimation of the orientations of shapes are illustrated by examples given in the following section.

5 Experiments

The first experiment applies the squareness measure to the classification of the MPEG-7 CE-1 database of 1400 shapes – see table 1. A set of five features had been previously been selected [19]: triangularity, roundness, rectangularity, ellipticity, and convexity,[1] which gave a score of 71.05% on the bulls-eye test when applied with a minimum Mahalanobis distance classifier; this is similar accuracy to other global descriptors [11] – see Zernike moments in table 1. If the shape measures are augmented by squareness $\mathcal{Q}_{\beta=2}(S)$ then the score improves to 72.97%. A better accuracy is provided by

Table 1 Bull's eye test scores for MPEG-7 CE-1 database. Values in the middle section are taken from [11].

method	score
5 shape features	71.05
5 shape + $\mathcal{Q}_{\beta=2}(S)$	72.97
5 shape + $\mathcal{Q}_{fit}(S)$	73.76
5 shape + $\mathcal{Q}_{\beta=2}(S) + \mathcal{Q}_{fit}(S)$	74.74
directed acyclic graph	60.00
wavelets	67.76
Zernike moments	70.22
multilayer eigenvectors	70.33
scale space	75.44
correspondence of visual parts	76.45
shape context [2]	76.51
inner distance shape context [12]	85.40
curvature tree [1]	87.13

including $\mathcal{Q}_{fit}(S)$ instead: 73.76%. Combining both along with the set of five features produces a further improvement in accuracy (74.74%), showing that the two squareness measures are providing mostly independent information. This is also shown when just the squareness measures are used without the other five shape features. Accuracies are $\mathcal{Q}_{\beta=2}(S)$: 23.07%, $\mathcal{Q}_{fit}(S)$: 23.00% and the two combined gives 39.60%. We note that it is possible to obtain significantly better bull's eye scores, as demonstrated by state of the art methods such as that by Alajlan *et al.* [1] which achieves 87.13%. They use a curvature tree to model the shape and topology of objects, and perform dynamic space warping and the Hungarian bipartite matching algorithm to enable exact tree matching. A drawback with such approaches is that computational complexity increases, as does the difficulty in implementation. In Alajlan *et al.*'s method construction of the tree from a shape containing N boundary points is $O(N^2)$, and matching between two trees is $O(bnmN^2)$, where b is the maximum branching factor and the trees contain n and m nodes respectively. Another example is the inner distance shape context of Ling and Jacobs [12], for which construction of the descriptor for one shape is $O(N^3)$ and matching two shapes requires $O(N^2)$ time. A great advantage of global descrip-

---

[1] The specific shape measures used were: a Fourier based triangularity measure [3], roundness based on the ratio of the areas of the shape S and its circumscribing circle, rectangularity based on the ratio of the areas of the shape S and its minimum bounding rectangle, ellipticity based on the first affine moment invariant [17] and convexity based on the areas of the shape S and its convex hull.
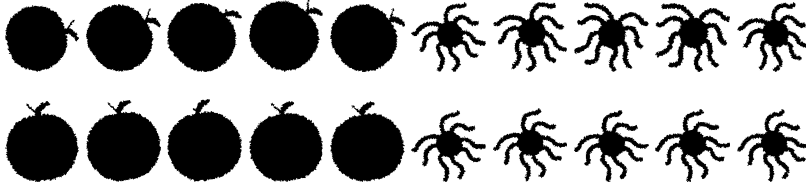
Fig. 9 Original data with added noise; upper row orientated using moments, lower row orientated using squareness ($\beta = 8$).

tors such as ours is that the computational cost of using them for matching shapes is independent of the number of boundary points.

Table 2 Circular variance of orientation estimates for 10 noisy shape instances, averaged over 1400 shapes from MPEG-7 CE-1 database. The rows show results for different normalisations and scalings (in the X direction) of the data before noise is added.

data	moments	$\mathcal{Q}_{fit}(S)$	squareness $\mathcal{Q}_\beta(S)$						$\mathcal{R}_{\beta=8}^{\delta=50}(S)$
			$\beta = 0.5$	$\beta = 1$	$\beta = 2$	$\beta = 4$	$\beta = 8$	$\beta = 16$	
original	0.0416	0.0830	0.0395	0.0390	0.0373	0.0356	**0.0322**	0.0373	**0.0231**
normalised	0.4592	0.1181	0.0478	0.0480	0.0448	0.0455	**0.0440**	0.0510	**0.0473**
normalised; $X_s = 1.01$	0.2969	0.1194	0.0494	0.0503	0.0451	0.0429	**0.0400**	0.0498	**0.0298**
normalised; $X_s = 1.10$	0.0201	0.0962	0.0393	0.0386	0.0414	0.0333	**0.0210**	0.0289	**0.0130**
normalised; $X_s = 1.25$	0.0094	0.0797	0.0327	0.0327	0.0337	0.0200	**0.0147**	0.0197	**0.0071**

For the next experiment we also used the MPEG-7 CE-1 database, but in this case to test the effectiveness of squareness for determining shape orientation. There are no ground-truth "correct" orientations for the shapes. In practise what is required is a means for standardising the orientation of each shape in a consistent manner so that the pose of unseen objects can be set prior to matching against the dataset of models. Therefore we test effectiveness of the orientation estimators by measuring their stability under relatively small changes to the shapes. Shape orientations were computed using $\mathcal{Q}_\beta(S)$ and $\mathcal{Q}_{fit}(S)$ by determining the orientations that minimised the integral in (19) and the intersection area in (1) respectively. In addition the principal axis method, determined from the shape's moments [24] was applied; this method will be referred to as the 'moment based' method and is probably the most standard method for computing orientation.

Noise was added to the shapes as follows: points on the boundary were perturbed in their normal direction with random magnitude determined by a Normal distribution with standard deviation of 4. The X and Y extents of the shapes are typically in the range [300,500]. A morphological opening with circular structuring element of diameter 3 was applied to tidy up the shape, following which only the largest connected component was retained. The latter step occasionally removes narrow parts of the shape, which can also be considered to be a typical segmentation error.
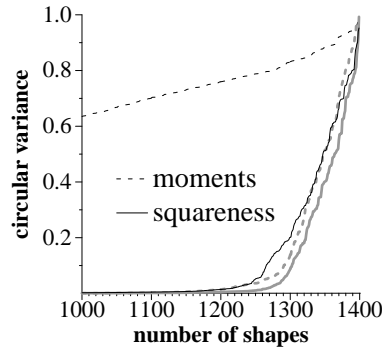
Fig. 10 Sorted circular variances of orientation estimates plotted for the 400 shapes with the highest variances. Gray curves (rightmost curves on graph) represent variances on the noisy versions of the original MPEG-7 CE-1 data and black curves represent variances on the noisy versions of the normalised data.

Fig. 11 Normalised data with added noise; upper row orientated using moments, lower row orientated using squareness ($\beta = 8$).

Ten noisy versions of each shape were generated, and the circular variance (which is in the range [0,1]) [13] of the ten estimated orientations was calculated, where orientations modulo $90°$ were used. Table 2 lists the mean circular variances averaged over all 1400 shapes. We note that for the squareness method the value of 8 is a good choice for β across the different versions of MPEG-7 CE-1 database. This can be considered to be the best trade off between increasing β so as to increase $\mathcal{Q}_\beta(S)$'s sensitivity to small deviations so that difficult (e.g. compact) shapes can be oriented, whilst avoiding increasing β so much that $\mathcal{Q}_\beta(S)$ becomes over-sensitive to noise. Thus, if the test set had contained a different level of noise then a different value of β would be appropriate. It can be seen that, even on the original data, overall the squareness based orientation is slightly better than the moment based approach. Although the moment based approach is generally effective for many of the shapes, especially those that are elongated, there are also many other shapes contained in the MPEG-7 CE-1 database that are problematic. Some of those are symmetric shapes such as stars, squares, and other rotationally symmetric shapes. Others are compact such as the apple in figure 9. However, it is obviously still potentially orientable, and it can be seen that squareness is successful in doing so. The octopus in figure 9 is neither rotationally symmetric or compact, but again orientation computed by squareness is much more consistent than that by moments.

The performance of the orientation estimators is further explored by normalising the data following the approach of Süße and Ditrich [26] in which a shearing and anisotropic scaling is applied to produce a shape that is unorientable by the moments based method. However, as can be seen from table 2 the mean circular variance of

Fig. 12 Normalised data with a 1.1 scale factor in X and added noise; upper row orientated using moments, lower row orientated using squareness ($\beta = 8$).

the moments based method is still below unity (i.e. its performance is better than random) since the process of adding noise makes some of the shapes more orientable. Nevertheless, whereas most of the shapes are consistently oriented by both of the methods for the original data, with the normalised data the variances for the moments based method are roughly uniformly distributed in [0,1] while the squareness method is only slightly affected; see figure 10. We note that the MPEG-7 CE-1 database contains shapes such as stars with high orders of rotational symmetry (e.g. 8) that have intrinsic ambiguity if orientations modulo $90°$ are used. This leads to the small proportion of shapes that have high variances for both methods even before the normalisation step. Examples of the moments based method producing inconsistent orientation estimates on the normalised data are given in figure 11. For both shapes the squareness method is very consistent.

When the normalised data is stretched to make it more elongated then it naturally becomes more orientable, and the circular variances reduce (see table 2). Rescaling all the data by 1.1 in the X direction ensures that even the previously problematic shapes (such as the symmetric shapes) are now orientable by the moments based method. Additional elongation further reduces the circular variances of the moments based method. In contrast, the squareness method is already consistent for compact shapes, and unlike the moments based method its circular variance does not decrease as substantially for elongated shapes. The moments based method can generally determine orientations reliably for the elongated shapes produced after the data is scaled in X by 1.1. However, even for such shapes the noise model used to generate the data can still cause problems. Figure 12 shows an example in which the thin parts of the rat (tail, feet, etc.) are prone to truncation when noise is added. It can be seen that the orientations estimated by the moments based method are more prone to disruption than those of the squareness method.

The square fitting method $\mathcal{Q}_{fit}(S)$ provides similar advantages to $\mathcal{Q}(S)$ for the normalised data and also the close to normalised data (i.e. scaling in the X direction by 1.01). However, it is consistently outperformed by the moments based method in all other situations. Moreover, $\mathcal{Q}(S)$ produces better results than $\mathcal{Q}_{fit}(S)$ for *all* versions of the dataset.

Furthermore, the version of $\mathcal{Q}(S)$ generalised to provide a rhomboidal measure provides further improvements, yielding more reliable orientation estimates for all the sets of database scalings except for the normalised data (i.e. the most extreme case). Even for the latter case only a small increase in error occurs. As shown in table 2, $\mathcal{R}_{\delta}^{\beta}(S)$ consistently outperforms both the moments based method and $\mathcal{Q}_{fit}(S)$, even
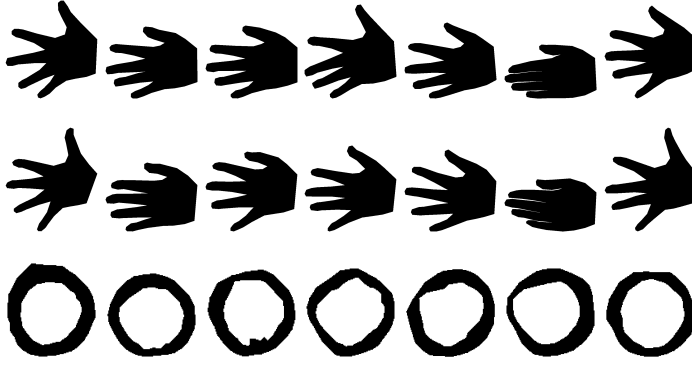
Fig. 13 Seven examples of shape data from sequences of deforming objects after landmark based pose normalisation.

for the largest scaling of the data $X_s = 1.25$ for which all the shapes are distinctly elongated.

Table 3 Circular variance of orientation estimates for data sequences shown in figure 13.

data	moments	squareness						
		$\beta = 0.5$	$\beta = 1$	$\beta = 2$	$\beta = 4$	$\beta = 8$	$\beta = 16$	$\beta = 32$
hand (1)	0.1619	0.1819	0.2267	0.3727	0.2841	**0.0808**	0.0585	0.0844
hand (2)	0.3068	0.2905	0.3219	0.3256	0.3214	**0.2415**	0.2193	0.1767
ventricle	0.7948	0.3806	0.3723	0.3486	0.2480	**0.1987**	0.2041	0.2509

The second experiment on orientation tests the stability of the orientation estimates in a different way. A sequence of instances of a deforming object are used – despite the shape differences the aim is to consistently orient the shapes within the sequence. The data was provided by the Technical University of Denmark for the purpose of building statistical shape models, and consists of a set of landmarks which correspond over the shape sequence. Given such a point correspondence it is straightforward to estimate a similarity transformation to normalise the pose of the shapes. Following Cootes *et al.* [6] the best transformation, in the least squares sense, is determined for each shape against one arbitrary shape which is chosen as the reference. The mean of the transformed shapes becomes the reference shape, and this process is iterated until convergence.

This pre-normalisation acts as a sort of ground-truthing, enabling us to assess the orientation estimates by their circular variances in the same manner as the first experiment. However, in this case the shape variations are more natural – although more severe – compared to the addition of synthetic noise. Figure 13 shows example shapes from each sequence; the two hand sequences each contain 20 frames, while the bottom sequence contains 14 left ventricles from cardiac MR images. Again, table 3 demonstrates that the squareness based orientations with $\beta = 8$ are more consistent than the moment based orientation. In fact, for the hand sequences further improvements are obtained by increasing the value of β to $\beta = 16$. All the circular variances are higher

than in the previous experiment with the MPEG-7 CE-1 database which is due to the greater variability of the shapes compared with just uniformly adding noise. Also, as expected, the compact shape of the ventricle is especially difficult, but while the moment based method fails the squareness based method performs reasonably well.

6 Conclusion

This paper has described a measure to quantify the degree to which a shape is square-like. There appears to be little in the literature on methods to measure squareness, but some general methods for defining shape descriptors can be adopted to test shape squareness. A standard approach to defining shape descriptors is used here for comparison in testing the performance of the new squareness measures. We note that one of reasons for a lack of methods for measuring the squareness of shapes could be the fact that there is no 'simple' equation of the square boundary (e.g. the existence of such an equation leads to straightforward methods for measuring shape circularity). Another reason is that a square has no straightforward geometric property which could lead to a simple definition of the shape squareness measure. In comparison, simple definitions of the convex shapes have led to several definitions for shape convexity measures [4, 10, 16, 20, 21, 25, 29].

Roughly speaking, we start from the integral $\iint_S(|x| + |y|)dxdy$ and show that it reaches the minimal possible value if and only if S is a square which is suitably oriented. Such a minimum is $\sqrt{2 Area(S)^3}/3$. Based on this we define the shape squareness measure as

$$\mathcal{Q}(S) \;=\; \frac{\sqrt{2}}{3} \cdot \frac{Area(S)^{3/2}}{\min\limits_{\alpha \in [0,2\pi]} \int\int\limits_{S(\alpha)}(|x| + |y|)dxdy},$$

where S is the measured shape and $S(\alpha)$ is obtained by rotating S around the origin for an angle α. In order to extend the number of applications where the squareness measure could be a useful tool we generalise the definition of $\mathcal{Q}(S)$ and come to the definition $\mathcal{Q}_\beta(S)$ of the shape squareness which takes into account relative positions of points inside the shape. $\mathcal{Q}_\beta(S)$ is defined as:

$$\mathcal{Q}_\beta(S) = \begin{cases} \dfrac{2^{1-\beta/2} Area(S)^{1+\beta/2}}{(2+\beta) \min\limits_{\alpha \in [0,2\pi]} \iint_{S(\alpha)}(|x| + |y|)^\beta dxdy}, & \beta > 0 \\[4mm] \dfrac{(2+\beta) \max\limits_{\alpha \in [0,2\pi]} \iint_{S(\alpha)}(|x| + |y|)^\beta dxdy}{2^{1-\beta/2} Area(S)^{1+\beta/2}}, & \beta \in (-1, 0) \end{cases}$$

Both measures $\mathcal{Q}(S) = \mathcal{Q}_{\beta=1}(S)$ and $\mathcal{Q}_\beta(S)$ have the following desirable properties:
- easy to compute;
- area based, and therefore robust;
- range in $(0, 1]$;
- maximised only by a square;
- invariant to similarity transformations;
- applicable to compound shapes, as well;
- naturally defined and theoretically well founded;
- results match human intuition.

In addition, the orientation of the shape that maximises the squareness measure has been shown to be a reliable estimator of the shape's orientation, while $\mathcal{R}(S)$, a modified version of $\mathcal{Q}(S)$ that provides a rhomboidal measure, was found on the MPEG-7 CE-1 database to provide even more reliable orientation estimates. Unlike the standard principal axis method $\mathcal{Q}(S)$ and $\mathcal{R}(S)$ are able to cope even with shapes that are compact and/or symmetric.

The behaviour of the introduced squareness measures and their usefulness, together with applicability to the computing of shape orientation, is verified on three large shape databases: diatoms (ADIAC), MPEG-7 CE-1, and trademarks. The obtained results have shown the benefits of the new measures in the majority of performed experiments.

The proposed measure of squareness has been developed and defined in the continuous space. Therefore some of the measure's properties are only strictly true for continuous shapes. In practise, any discrepancies are insignificant except for very small shapes. A topic for future research would be to develop a measure of squareness defined on discrete data.

References

1. N. Alajlan, M.S. Kamel, and G.H. Freeman. Geometry-based image retrieval in binary image databases. *IEEE Trans. on Patt. Anal. and Mach. Intell.*, 30(6):1003–1013, 2008.
2. S. Belongie, J. Malik, and J. Puzicha. Shape matching and object recognition using shape contexts. *IEEE Trans. on Patt. Anal. and Mach. Intell.*, 24(4):509–522, 2002.
3. E.T. Bowman, K. Soga, and T. Drummond. Particle shape characterization using Fourier analysis. *Geotechnique*, 51(6):545–554, 2001.
4. L. Boxer. Computing deviations from convexity in polygons. *Pattern Recognition Letters*, 14:163–167, 1993.
5. D. Coeurjolly and R. Klette. A comparative evaluation of length estimators of digital curves. *IEEE Trans. on Patt. Anal. and Mach. Intell.*, 26(2):252–257, 2004.
6. T.F. Cootes, C.J. Taylor, D.H. Cooper, and J. Graham. Active shape models-their training and application. *Computer Vision and Image Understanding*, 61(1):38–59, 1995.
7. J.M.H. du Buf and M.M. Bayer, editors. *Automatic Diatom Identification*. World Scientific, 2002.
8. G.H. Granlund. Fourier preprocessing for hand print character recognition. *IEEE Trans. on Computers*, 21:195–201, 1972.
9. A.K. Jain and A. Vailaya. Shape-based retrieval: A case-study with trademark image databases. *Pattern Recognition*, 31(9):1369–1390, 1998.
10. R. Kakarala. Testing for convexity with Fourier descriptors. *Electronics Letters*, 34(14):1392–1393, 1998.
11. L.J. Latecki, R. Lakämper, and U. Eckhardt. Shape descriptors for non-rigid shapes with a single closed contour. In *Proc. Conf. Computer Vision Pattern Recognition*, pages 1424–1429, 2000.
12. H. Ling and D.W. Jacobs. Shape classification using the inner-distance. *IEEE Trans. on Patt. Anal. and Mach. Intell.*, 29(2):286–299, 2007.
13. K.V. Mardia and P.E. Jupp. *Directional Statistics*. John Wiley, 1999.
14. D.L. Page, A. Koschan, S.R. Sukumar, B. Roui-Abidi, and M.A. Abidi. Shape analysis algorithm based on information theory. In *Int. Conf. Image Processing*, volume 1, pages 229–232, 2003.
15. D. Proffitt. The measurement of circularity and ellipticity on a digital grid. *Pattern Recognition*, 15(5):383–387, 1982.

16. E. Rahtu, M. Salo, and J. Heikkilä. A new convexity measure based on a probabilistic interpretation of images. *IEEE Trans. on Patt. Anal. and Mach. Intell.*, 28(9):1501–1512, 2006.
17. P.L. Rosin. Measuring shape: Ellipticity, rectangularity, and triangularity. *Machine Vision and Applications*, 14:172–184, 2003.
18. P.L. Rosin. Computing global shape measures. In C.H. Chen and P.S.P. Wang, editors, *Handbook of Pattern Recognition and Computer Vision*, pages 177–196. World Scientific, 2005.
19. P.L. Rosin. A two-component rectilinearity measure. *Computer Vision and Image Understanding*, 109(2):176–185, 2008.
20. P.L. Rosin and C.L. Mumford. A symmetric convexity measure. *Computer Vision and Image Understanding*, 103(2):101–111, 2006.
21. P.L. Rosin and J. Žunić. Probabilistic convexity measure. *IET Image Processing*, 1(2):182–188, 2007.
22. P.L. Rosin and J. Žunić. 2d shape measures for computer vision. In A. Nayak and I. Stojmenovic, editors, *Handbook of Applied Algorithms: Solving Scientific, Engineering, and Practical Problems*, pages 347–372. Wiley, 2008.
23. N. Sladoje and J. Lindblad. High precision boundary length estimation by utilizing gray-level information. *IEEE Trans. on Patt. Anal. and Mach. Intell.*, 31(2):357–363, 2009.
24. M. Sonka, V. Hlavac, and R. Boyle. *Image Processing, Analysis, and Machine Vision.* Thomson-Engineering, 2007.
25. H.I. Stern. Polygonal entropy: a convexity measure. *Pattern Recognition Letters*, 10:229–235, 1989.
26. H. Süße and F. Ditrich. Robust determination of rotation-angles for closed regions using moments. In *Int. Conf. Image Processing*, volume 1, pages 337–340, 2005.
27. H. Zabrodsky, S. Peleg, and D. Avnir. Symmetry as a continuous feature. *IEEE Trans. on Patt. Anal. and Mach. Intell.*, 17(12):1154–1166, 1995.
28. J. Žunić and P.L. Rosin. Rectilinearity measurements for polygons. *IEEE Trans. on Patt. Anal. and Mach. Intell.*, 25(9):1193–1200, 2003.
29. J. Žunić and P.L. Rosin. A new convexity measurement for polygons. *IEEE Trans. on Patt. Anal. and Mach. Intell.*, 26(7):923–934, 2004.
30. J. Žunić, P.L. Rosin, and L. Kopanja. On the orientability of shapes. *IEEE Trans. on Image Processing*, 15(11):3478–3487, 2006.

7 Appendix

Proof of Lemma 3 Let S be a given shape different from a square. Let $K(a)$ be the square with $a = \sqrt{Area(S)}/2$ – i.e. the areas of S and $K(a)$ are the same. Because S and $K(a)$ are assumed to be different shapes then

$$\Delta = Area(S \setminus K(a)) = Area(K(a) \setminus S) > 0. \tag{23}$$

Further, let us define the parameter a_{ext} as follows:

$$a_{ext} = \sqrt{a^2 + \frac{\Delta}{2}}. \tag{24}$$

It is easy to check that such a defined parameter a_{ext} provides

$$Area(K(a_{ext}) \setminus K(a)) = \Delta. \tag{25}$$

Now, by using the same reasoning as in the proof of Theorem 1, assuming $\beta > 0$, and by using (24) we derive

$$\iint\limits_{S \setminus K(a)} (|x| + |y|)^\beta dxdy \ \geq \ \int\limits_{a \leq |x| + |y| \leq a_{ext}} \int (|x| + |y|)^\beta dxdy \tag{26}$$

$$= 4 \int_{x=0}^{a_{ext}} \left(\int_{y=0}^{a_{ext}-x} (x+y)^\beta dy \right) dx \quad - \quad 4 \int_{x=0}^{a} \left(\int_{y=0}^{a-x} (x+y)^\beta dy \right) dx \quad (27)$$

$$= \frac{4}{\beta+2} \left(a_{ext}^{\beta+2} - a^{\beta+2} \right) \tag{28}$$

$$= \frac{4}{\beta+2} \left(\left(a^2 + \frac{\Delta}{2} \right)^{(\beta+2)/2} - a^{\beta+2} \right) \tag{29}$$

$$= \frac{4a^{\beta+2}}{\beta+2} \left(\left(1 + \frac{\Delta}{2a^2} \right)^{(\beta+2)/2} - 1 \right) \tag{30}$$

Now, Taylor expression of $(1+x)^\alpha$ with $x = \dfrac{\Delta}{2a^2}$ and $\alpha = \dfrac{\beta+2}{2}$

implies a $\theta \in (0,1)$ such that

$$= \frac{4a^{\beta+2}}{\beta+2} \left(\frac{(\beta+2)\Delta}{4a^2} + \frac{\beta(\beta+2)}{8} \left(1 + \theta \frac{\Delta}{2a^2} \right)^{\frac{\beta+2}{2}\left(\frac{\beta+2}{2}-1\right)} \right) \tag{31}$$

$$\geq \frac{4a^{\beta+2}}{\beta+2} \cdot \frac{(\beta+2)\Delta}{4a^2} \tag{32}$$

$$= a^\beta \Delta \tag{33}$$

Notice that the last proved inequality:

$$\iint\limits_{S \backslash K(a)} (|x| + |y|)^\beta dxdy \; \geq \; a^\beta \Delta, \tag{34}$$

does not depend on how the shape S is rotated. In other words, if α_0 is the angle which minimises the integral $\iint_{S(\alpha)} (|x| + |y|)^\beta dxdy$ we have the estimate which is analogous to (32) and we can write:

$$\int\limits_{S(\alpha_0) \backslash K(a)} \!\!\!\! \int (|x| + |y|)^\beta dxdy \; \geq \; a^\beta \Delta \tag{35}$$

where

$$\int\limits_{S(\alpha_0) \backslash K(a)} \!\!\!\! \int (|x| + |y|)^\beta dxdy \; = \; \min_{\alpha \in [0, 2\pi]} \int\limits_{S(\alpha) \backslash K(a)} \!\!\!\! \int (|x| + |y|)^\beta dxdy. \tag{36}$$

Further, we derive

$$\mathcal{Q}_\beta(S) = \frac{2^{1-\beta/2} Area(S)^{1+\beta/2}}{(2+\beta) \min\limits_{\alpha \in [0, 2\pi]} \iint_{S(\alpha)} (|x| + |y|)^\beta dxdy} \tag{37}$$

$$= \frac{2^{1-\beta/2} Area(S)^{1+\beta/2}}{(2+\beta) \iint_{S(\alpha_0)} (|x| + |y|)^\beta dxdy} \tag{38}$$

$$\leq \frac{2^{1-\beta/2}Area(S)^{1+\beta/2}}{(2+\beta)\iint_{S(\alpha_0)\setminus K(a)}(|x|+|y|)^\beta dxdy} \tag{39}$$

$$\leq \frac{2^{1-\beta/2}Area(S)^{1+\beta/2}}{(2+\beta)a^\beta\Delta} \tag{40}$$

$$\leq \frac{2^{1-\beta/2}(2a^2)^{1+\beta/2}}{(2+\beta)a^\beta\Delta} \tag{41}$$

$$= \frac{4a^2}{(2+\beta)\Delta}. \tag{42}$$

Finally, taking into account that Δ and a are strictly positive, and do not depend on β, the last proven inequality $\mathcal{Q}_\beta(S) \leq \dfrac{4a^2}{(2+\beta)\Delta}$ gives the required: $\lim\limits_{\beta\to\infty}\mathcal{Q}_\beta(S) = 0$. $\square$